A dual-ligand liposomal system composed of a cell-penetrating peptide and a mitochondrial RNA aptamer synergistically facilitates cellular uptake and mitochondrial targeting

Yuma Yamada[1,2], Ryo Furukawa[1,2], and Hideyoshi Harashima[1,*]

[1] Laboratory for molecular design of pharmaceutics, Faculty of Pharmaceutical Sciences, Hokkaido University, Kita-12, Nishi-6, Kita-ku, Sapporo 060-0812, Japan.
[2] These authors equally contribute this study.

*Corresponding author: Laboratory for molecular design of pharmaceutics, Faculty of Pharmaceutical Sciences, Hokkaido University, Kita-12, Nishi-6, Kita-ku, Sapporo 060-0812, Japan
Tel: +81-11-706-3919 Fax: +81-11-706-4879
E-mail: harasima@pharm.hokudai.ac.jp

Keywords: targeted drug delivery; liposomes; aptamer; drug delivery systems; nanotechnology.

Abstract

It has been reported that the use of mitochondrial RNA aptamers including RNase P (RP) results in the selective mitochondrial delivery of endogenous and exogenous RNAs. The issue of whether these aptamers would be useful ligands for the mitochondrial targeting of a nanoparticle has not been demonstrated to date, because nanocarriers modified with these RNA aptamers are insufficiently internalized by cells. We report herein on the development of a dual-ligand liposomal system composed of octaarginine (R8), a device that enhances cellular uptake, and an RP aptamer for mitochondrial targeting to permit a nanocarrier to be efficiently delivered to mitochondria. Surprisingly, the cellular uptake of the R8-modified nanocarrier was facilitated by modification with an RP aptamer. The optimal composition of a nanocarrier needed for efficient cellular uptake and mitochondrial targeting was determined. In a confocal laser scanning microscopy analysis, the dual-ligand modified nanocarrier was found to result in effective mitochondrial targeting *via* an ATP dependent pathway and was much more effective than a single-ligand R8-modified nanocarrier. This is the first report of the regulation of intracellular trafficking by a mitochondrial RNA aptamer modified nanocarrier system.

1. Introduction

If it was possible to develop an active targeting system that could target a specific organelle, this would open a new field of research directed toward therapy for various diseases. Mitochondria are promising targets for delivering therapeutic molecules [1]. Mitochondrial dysfunctions are implicated in a variety of human diseases, including neurodegenerative disorders, ischemia reperfusion injury, cancer and inherited mitochondrial diseases [2-5]. Accordingly, it would be expected that delivering therapeutic molecules to mitochondria in diseased cells be a strategy for the treatment of mitochondrial dysfunctions, resulting in the suppression of mitochondrial related diseases.

The mitochondrial targeting signal peptide (MTS), which is necessary for targeting nuclear-encoded protein to mitochondria, is useful as a specific ligand for mitochondria [6,7]. Previous reports showed that the conjugation or direct modification of MTS permitted a macromolecule such as a protein, DNA and a liposomal nanocarrier to be delivered to mitochondria [8-12]. On the other hand, some researchers have reported the use of a mitochondrial RNA aptamer for mitochondrial delivery. The mitochondrial import of mitochondrial ribozyme, RNase P (RP) and mitochondrial RNase P (MRP) were reported to be mediated by polynucleotide phosphorylase (PNPase) [13]. Wang and coworkers showed that allotropically encoded mitochondrial mRNAs and tRNA were imported by RP and MRP aptamers into mitochondria [13,14]. Adhya and coworkers reported that the combination of a mitochondrial tRNA import signal (D-arm) and a RNA import complex (RIC), which were found in Leichmania tropica, induced the transport of tRNA and antisense RNA into mitochondria in living cells [15]. However, the direct modification of a mitochondrial RNA aptamer on a nanocarrier has not been a subject of extensive investigation.

The present study focused on enhancing mitochondrial targeting by modification of a liposomal based nanocarrier with a mitochondrial RNA aptamer. The mitochondrial RNA aptamers used in this study included RP and MRP, in which mitochondrial delivery occurs *via* PNPase [13], and the D-arm with a high affinity with the tubulin antisense binding protein (TAB) located on the mitochondrial outer membrane [16] (Table 1). These RNA aptamers themselves have mitochondrial targeting activity, but modifying the carrier with a single aptamer would not be sufficient to allow the particle to be internalized by a cell. We recently reported on the development of a mitochondrial delivery system, a MITO-Porter in which the surface is modified with octaarginine (R8). The R8 functions as both a cellular uptake device *via* macropinocytosis and as a mitochondrial targeting peptide *via* electrostatic interactions

with negatively charged mitochondria [17-19]. We also developed a dual-ligand system in which the nanocarrier is modified with a specific ligand and R8 [20,21]. These systems have a synergistic effect on both selectivity and cellular uptake.

Thus, we expected that a dual-ligand liposomal system modified with both R8 and a mitochondrial RNA aptamer would show an enhanced mitochondrial delivery. In this study, we prepared a dual-ligand modified MITO-Porter composed of R8 with different amounts of mitochondrial RNA aptamers including RP, MRP and the D-arm. We then evaluated the cellular uptake efficiency of the carriers using flow cytometry. The extent of intracellular trafficking was observed by confocal laser scanning microscopy (CLSM), and the mitochondrial targeting rate and mitochondrial occupancy rate were estimated based on the obtained CLSM images.

2. Materials and Methods

2.1. Chemicals and materials

1,2-dioleoyl-*sn*-glycero-3-phosphoethanolamine (DOPE), sphingomyelin (SM), and DOPE-N-(7-nitro-2-1,3-benzoxadiazole-4-yl) (NBD-DOPE) were purchased from Avanti Polar lipids (Alabaster, AL). Stearylated R8 (STR-R8) [22] was obtained from KURABO Industries (Osaka, Japan). Cholesterol covalently linked to the 3′ end of 2′-O-Methyl RNAs (Chol-RNA aptamer) containing the RP sequence (Chol-RP), MRP sequence (Chol-MRP) and the D-arm sequence (Chol-D-arm) were obtained from Hokkaido System Science Co., Ltd. (Sapporo, Japan). The sequences of the RNA aptamers in these cholesterol derivatives are summarized in Table 1. HeLa human cervix carcinoma cells were obtained from the RIKEN Cell Bank (Tsukuba, Japan). Dulbecco's modified Eagle medium (DMEM) and fetal bovine serum were purchased from Invitrogen (Carlsbad, CA). Amirolide, filipin III, carbonyl cyanide 4-(trifluoromethoxy) phenylhydrazone (FCCP) and oligomycin were purchased from SIGMA (St Louis, MO). All other chemicals used were commercially available reagent-grade products.

2.2. Preparation of dual-ligand modified MITO-Porter

Dual-ligand modified MITO-Porter was constructed by the hydration method [17]. A lipid film was formed by the evaporation of a chloroform/ethanol solution containing DOPE/SM/NBD-DOPE (9:2:0.1, molar ratio). NBD-DOPE was added to the lipid composition as a tracer for the MITO-Porter. To prepare the dual-ligand modified MITO-Porter, 1-4 mol% of Chol-RNA aptamers were added to the lipid composition. The 10 mM 4-(2-hydroxyethyl)-1-piperazineethanesulfonic acid (HEPES) buffer (pH

7.4) was applied to the lipid film, followed by incubation for 15 min at room temperature to hydrate the lipids. The lipid film was sonicated for approximately 1 min in a bath-type sonicator. An STR-R8 solution (10 mol% total lipid) was added to the suspension to attach the R8 to the surface.

2.3. Characterization of prepared carriers

Particle diameters were measured using a dynamic light scattering (DLS) method (Zetasizer Nano ZS; Malvern Instruments, Worcestershire, UK). Samples were prepared in 10 mM HEPES buffer at 25°C and the values of particle diameters are shown in the form of volume distribution. The ζ-potentials of samples were also determined in 10 mM HEPES buffer at 25°C using a Zetasizer Nano ZS.

2.4. Cell cultures

HeLa cells were maintained in complete medium, which is DMEM supplemented with 10% FBS, penicillin (100 units/mL), and streptomycin (100 μg/mL). The cells were cultured under an atmosphere of 5% CO_2/air at 37°C. One day before transfection, the HeLa cells were seeded on plates or dishes for each experiment. Immediately before transfection, the medium was replaced to serum-free medium, DMEM unsupplemented with antibiotics.

2.5. Cellular uptake analysis using flow cytometry

NBD-DOPE labeled MITO-Porter (8.25 nM of total lipids) was incubated with HeLa cells (5 x 10^4 cells/dish) seeded on 12-well plate (BD Falcon; Becton Dickinson, Franklin Laynkes, NJ) in 1 mL of serum free DMEM, under an atmosphere of 5% CO_2 / air at 37ºC for 3 hr. After the incubation, the cells were washed once with ice-cold phosphate-buffered saline (PBS), and then twice with ice-cold PBS containing heparin (20 U/mL) and trypsinized. After adding complete medium, the cell suspension was centrifuged (800*g*, 4°C, 5 min) and the resulting pellet was suspended in PBS containing 0.5% bovine serum albumin, and 0.1% sodium azide. The cell suspension was filtered through a nylon mesh followed by analysis by flow cytometry (FACScan, Becton Dickinson). NBD was excited at a wavelength of 488 nm and the fluorescence detection channel was set to an FL1 filter for NBD. Cellular uptake was expressed as the mean fluorescence intensity (MFI), calculated using the CellQuest software (Becton Dickinson). A total of 10,000 cells were analyzed in each sample.

To investigate the mechanism responsible for the cellular uptake of carriers, the cells were incubated with carriers in the presence of inhibitors. The cells were treated

with inhibitors (0.3 M sucrose, 5 mM amiloride, and 15 μM filipin III, 100 nM FCCP and 10 nM oligomycin) for 1 hr before adding the carriers to the cells. The relative cellular uptake when the cells were treated with inhibitors was calculated as follows;
Relative cellular uptake value (%) = $U_P/U_A \times 100$
where U_P and U_A represent the cellular uptake of the NBD labeled carriers when cells were treated with carriers in the presence and absence of inhibitors, respectively.

2.6 Intracellular observation of carrier using CLSM

NBD-DOPE labeled MITO-Porter (22 nM) was incubated with HeLa cells (1 x 10^5 cells/dish) seeded on 35 mm dishes (IWAKI, Osaka, Japan) in 1 mL of serum free DMEM, under an atmosphere of 5% CO_2 / air at 37ºC for 3 hr. Thirty minutes before acquiring the fluorescence images, the mitochondria were stained with Mitofluor 589 (Invitrogen) (final concentration, 100 nM). After the incubation, the cells were washed with serum free DMEM, and then observed by CLSM (FV10i-LIV; Olympus Corporation, Tokyo, Japan). The cells were excited with a 473 nm light and 559 nm light from an LD laser. Images were obtained using an FV10i-LIV equipped with a water-immersion objective lens (UPlanSApo 60x/NA. 1.2) and a dichroic mirror (DM405/473/559/635). The two fluorescence detection channels (Ch) were set to the following filters: Ch1: 490/50 (green) for NBD-labeled liposome, Ch2: 570/50 (red) for Mitofluor 589. To investigate the mechanism responsible for the mitochondrial targeting of the carriers, the cells were incubated with carriers in the presence of FCCP (a mitochondrial uncoupler to decrease mitochondrial membrane potential) or oligomycin (an ATPase inhibitor to stop ATP synthase). The cells were treated with 100 nM FCCP or 10 nM oligomycin were treated at 1 hr before adding the carriers to the cells.

2.7 Evaluation of mitochondrial targeting and mitochondrial occupancy based on CLSM images

Mitochondrial targeting and the mitochondrial occupancy of carriers were evaluated using Image Pro-Plus (Ropper Industries, Sarasota, FL), as described below. Fluorescent and bright-field cell images, after treatment with NBD labeled carriers (green), followed by staining mitochondria red, were captured by means of CLSM, as shown in Figure 3. Each eight-bit TIFF image was analyzed to quantify the total area of each region of interest. The yellow pixel areas where carriers (green) were co-localized with stained mitochondria (red) are marked in each image. The yellow, green and red pixel areas of each cluster in the cell, s_i(yellow), s_i(green) and s_i(red), were separately summed for each image, and are denoted as $S'_{z=j}$ (yellow), $S'_{z=j}$ (green) and $S'_{z=j}$ (red),

respectively. The values of $S'_{z=j}$ (yellow), $S'_{z=j}$ (green) and $S'_{z=j}$ (red) in each image were further summed and are denoted as S(yellow), S(green) and S(red), respectively. S(yellow), S(green) and S(red) represent the total area of carriers that were colocalized with the mitochondria, all of the carriers inside the cell and the mitochondrial region in the total cell. Mitochondrial targeting rate (Figure 4B) was calculated as follows;

Mitochondrial targeting rate (%) = S (yellow) / (S (yellow) + S (green)) × 100 (1)

This value indicates the rate at which carriers become colocalized with mitochondria of all carriers taken up by the cell, and is used to evaluate the mitochondrial targeting activity of the carriers. The relative mitochondrial targeting rate (Figures 5A(e), 5B(e)) was also calculated as follows;

Relative mitochondrial targeting rate (%) = T_P / T_A x 100 (2)

where T_P and T_A represent the mitochondrial targeting rate when cells were treated with carriers in the presence and absence of FCCP (Figure 5A(a-d)) or oligomycin (Figure 5B(a-d)), respectively.

Mitochondrial occupancy rate (Figure 4C) was calculated as follows;

Mitochondrial occupancy rate (%) = S (yellow) / S (red) × 100 (3)

This value indicates the rate that the carriers accumulated with mitochondrial region of total mitochondrial region in cell, and is used to evaluate the accumulation of the carriers in mitochondria.

2.8 Statistical Analysis

Each of the values shown in Table 2 represent the mean ± S.D (n=3). Data shown in Figures 1, 2, 5A (e), 5B (e) and 6 are expressed as the mean ± SEM for the indicated number of experiments. In Figures 4B and 4C, individual data are represented as circles, and the means (n=32-39) are indicated by bars. In Figure 1A and 6, the statistical significances between two groups were examined by the unpaired student's *t*-test. In Figure 2, 4B and 4C, we performed one-way ANOVA followed by bonfferoni test for multiple comparisons. In Figure 1B, 5A (e) and 5B (e), we performed two-way ANOVA analysis followed by bonferroni test to compare the effect of two factors. If a significant interaction between the two factors was found, a simple main effect test also performed. Levels of $P < 0.05$ were considered to be significant.

3. Results

3.1. Construction of dual-ligand modified MITO-Porter

Chol-RNA aptamers, including RP, MRP and the D-arm, were used to prepare

the dual-ligand modified MITO-Porter (RP/R8-modified MITO-Porter, MRP/R8-modified MITO-Porter and D-arm/R8-modified MITO-Porter). Information regarding the RNA aptamers used in this study is shown in Table 1. The physicochemical properties of the prepared carriers are summarized in Table 2. Their diameters were approximately 100-150 nm. Modification of a negatively charged RNA aptamer on the positively charged R8-modified MITO-Porter reduced the ζ-potentials from a positive charge to a negative charge, and the values became saturated when the modification ratio of RNA-aptamer exceeded 2.5 mol% of the total lipids. These results indicate that it is possible to attach the mitochondrial RNA aptamer to the surface of the R8-modified MITO-Porter.

3.2. Effect of the mitochondrial RNA aptamer modification on the cellular uptake of R8-modified MITO-Porter

We investigated the effect of mitochondrial RNA aptamer modification on the cellular uptake of the R8-modified MITO-Porter. Figure 1 shows data for the cellular uptake value of the NBD-labeled MITO-Porter. Without modification with the RNA aptamer, the use of R8 enhanced the cellular uptake of carriers (Figure 1A), as previously reported [7]. The cellular uptake values for the R8-modified MITO-Porter equipped with RP, MRP, the D-arm (closed columns) and R8-unmodified ones (open columns) are summarized in Figure 1B. The cellular uptake of the R8-modified MITO-Porter was enhanced by modification with the RNA aptamer, while the single modification of the RNA aptamer on R8-unmodified MITO-Porter had no effect on cellular uptake.

We also performed a two-way ANOVA analysis to compare the two factors that are “aptamer type” and “modification ratio of the R8 / RNA aptamer”. As a result, 1 mol% and a 2.5 mol% modification of RNA aptamers on the R8-modified MITO-Porter significantly increased in the cellular uptake values compared with the R8-unmodified MITO-Porter among “modification ratio of R8/aptamer” ($^{###}P < 0.001$). No significant difference in different “aptamer type” on the cellular uptake value ($P = 0.21$) and no interaction between two factor ($P = 0.14$) was found, suggesting that the enhancement in the cellular uptake of the R8-modified MITO-Porter by the modification with the RNA aptamer would be independent on “aptamer type”. The 2.5 mol% modification with RP on the R8-modified MITO-Porter indicated the highest cellular uptake value among all variants of the MITO-Porter. For the following studies, 2.5 mol% RNA aptamer was modified on the surface of the R8-modified MITO-Porters.

3.3. Investigation of the cellular uptake pathway of dual-ligand modified MITO-Porter

To investigate whether the modification with a RNA aptamer affects the cellular uptake pathway of the R8-modified MITO-Porter, cellular uptake was evaluated in the presence of cellular uptake inhibitors (Figure 2). A hypertonic medium (sucrose) was used to inhibit clathrin-mediated endocytosis *via* the dissociation of the clathrin lattice [23]. Amiloride inhibits mactopinocytosis by inhibiting the Na^+/H exchange required for macropinocytosis [24]. Filipin III inhibits caveolar uptake through cholesterol depletion [25]. HeLa cells were incubated with the NBD-labeled R8-modified MITO-Porter (Figure 2A), the RP/R8-modified MITO-Porter (Figure 2B), the MRP/R8-modified MITO-Porter (Figure 2C), the D-arm/R8-modified MITO-Porter (Figure 2D) in the absence (closed bars) and presence (open bars) of the above inhibitors.

The cellular uptake for all types of dual-ligand modified MITO-Porters were significantly inhibited by sucrose and amiloride, indicating that the RNA aptamer/R8-modified MITO-Porters are mainly internalized into cells *via* clathrin-mediated endocytosis and macropinocytosis. A similar tendency of this cellular uptake pathway was also observed in the case of the R8-modified MITO-Porter, suggesting that RNA aptamer modification had a negligible effect on the cellular uptake route of R8-modified MITO-Porter **(**Figure 2**)**. These results suggest that the cell uptake route of dual-ligand modified MITO-Porter is dependent on R8.

3.4. Evaluation of the mitochondrial targeting activity of the dual-ligand modified MITO-Porter

The intracellular trafficking of the NBD-labeled R8-modified MITO-Porter and the dual-ligand modified MITO-Porter (RP/R8-modified MITO-Porter, MRP/R8-modified MITO-Porter and D-arm/R8-modifiedMITO-Porter) was observed using CLSM, as shown in Figure 3. In the case of the dual-ligand modified MITO-Porter, numerous yellow dots were observed in cells, indicating that the green fluorescence-labeled MITO-Porters were mainly localized in red-stained mitochondria (Figures 3B-D). On the other hand, numerous green dots were observed in the case of R8-modified MITO-Porter treatment, suggesting that the R8-modified MITO-Porter was partially localized in mitochondria (Figure 3A).

The mitochondrial targeting rate and mitochondrial occupancy rate were estimated based on the CLSM image shown in Figure 3 (Figure 4). Mitochondrial targeting rate indicates the carriers that are colocalized with mitochondria of all carriers taken up by the cell, and is used to evaluate the mitochondrial targeting activity of the

carriers. The dual-ligand modified MITO-Porter showed a higher mitochondrial targeting rate than that for the R8-modified MITO-Porter (Figure 4B). The mitochondrial occupancy rate of each carrier was also calculated. This value indicates that the carriers accumulated within the mitochondrial region of the total mitochondrial region in the cell, and is used to evaluate the mitochondrial accumulation of the carriers. As shown in Figure 4C, the values for the dual-ligand modified MITO-Porter were higher than that for the R8-modified MITO-Porter with a similar mitochondrial targeting rate. The RP/R8-modified MITO-Porter showed the highest mitochondrial targeting rate (Figure 4B) and mitochondrial occupancy (Figure 4C) among other dual-ligand modified MITO-Porters. Thus, the RP/R8-modified MITO-Porter was used in the following experiments as an optimal dual-ligand modified MITO-Porter.

3.5 Investigation of the mitochondrial targeting manner of dual-ligand modified MITO-Porter.

To investigate the effect of mitochondrial membrane potential on the mitochondrial targeting of the RP/R8-modified MITO-Porter and the R8-modified MITO-Porters, the intracellular trafficking of the carriers was observed in the presence/absence of FCCP (Figures 5A, S1). FCCP, an uncoupling regent, is a proton ionophore that depolarizes the mitochondrial membrane potential [26]. In the FCCP treatment, only green dots were observed in cells in the case of the RP/R8-modified MITO-Porter (Figure 5A (d)) and the R8-modified MITO-Porter (Figure 5A (c)).

The relative mitochondrial targeting rates were estimated based on the CLSM image shown in Figure 5A (a-d), and a two-way ANOVA analysis was performed to compare the effect of the two factors, i.e., the “carrier type” and the “FCCP treatment” (Figure 5A (e)). Significant differences were detected between presence and absence of FCCP ($P < 0.001$), while there was no significant difference for the different “carrier type” ($P = 0.72$) and no interaction between two factors ($P = 0.72$). These analytical results indicate that mitochondrial targeting of both the RP/R8 modified MITO-Porter and the R8-modified MITO-Porter was drastically inhibited when the cells were treated with FCCP.

We also evaluated the effect of ATP depletion on mitochondrial targeting using oligomycin (Figures 5B, S2), an inhibitor of ATP synthase that functions by blocking the proton channel (F_o subunit) for the oxidative phosphorylation of ADP to ATP [27]. In this experiment the RP/R8-modified MITO-Porter was observed as green dots in cells (Figure 5B (d)), while the R8-modified MITO-Porter was observed as yellow dots in the oligomycin treatment experiment (Figure 5B (c)).

In Figure 5B (e), the relative mitochondrial targeting rates were evaluated and two-way ANOVA analysis was performed. There were significant difference between the different "carrier type" ($P < 0.01$) and with/without "oligomycin treatment" ($P < 0.001$), and also a significant interaction between two factors ($P < 0.01$). The use of a simple main effect test indicated the existence of significant differences between the presence and absence of oligomycin in the case of both carriers (***$P < 0.001$), suggesting that ATP depletion affects the mitochondrial targeting of the RP/R8 and the R8 modified MITO-Porter. We also detected a significant difference between the R8-modified MITO-Porter and the RP/R8-modified MITO-Porter with an "oligomycin treatment" (***$P < 0.001$), suggesting that the mitochondrial targeting of the RP/R8-modified MITO-Porter was significantly decreased by ATP depletion compared with the R8-modified MITO-Porter.

Moreover, we investigated the cellular uptake of the carriers in the presence of FCCP and oligomycin. The cellular uptake of the RP/R8-modified MITO-Porter was drastically decreased to about 20 % as the result of the FCCP treatment, while that of the R8-modified MITO-Porter was not affected by FCCP treatment (Figure 6A). These results indicate that the RP/R8-modified MITO-Porter also functions *via* a mitochondrial membrane potential dependent cellular uptake pathway. In the oligomycin treatment, the effectiveness of both the RP/R8-modified MITO-Porter and the R8-modified MITO-Porter was decreased to about 70 % (Figure 6B). Both carriers are internalized into cells mainly *via* macropinocytosis and endocytosis (Figure 2), processes that require ATP, thus ATP depletion would affect cellular uptake.

4. Discussion

The present study focused on strategies for enhancing mitochondrial targeting by modification of a liposomal based nanocarrier with a mitochondrial RNA aptamer. To evaluate the targeting of the nanocarrier to mitochondria in living cells, we developed a dual-ligand system, in which the nanocarrier is modified with a mitochondrial RNA aptamer and R8. We expected that R8, which is reported to function as a cellular uptake device for a liposomal carrier [17-19], would assist the cellular internalization of the RNA aptamer-modified MITO-Porter with poor cellular uptake activity. The findings indicate, however, that "cellular uptake" and "mitochondrial targeting" between dual ligand-modified MITO-Porter and R8-modified MITO-Porter occur in significantly different manners. This aspect is discussed in detail.

In the cellar uptake analysis shown in Figure 1, modification of R8-modified MITO-Porter with the RNA aptamer enhanced the cellular uptake. The value of 2.5

mol% RP/R8-modified MITO-Porter (about 56 cellular uptake value) was 2 fold higher than that for the R8-modified MITO-Porter (about a 28 cellular uptake value). On the other hand, a single modification of the carrier with the RNA aptamer had essentially no effect on cellular uptake. The findings also confirmed that the cellular uptake of the dual-ligand modified MITO-Porter proceeded mainly *via* the R8-mediated pathway including clathrin mediated endocytosis and macropinocytosis, as shown in Figure 2. Based on these results, we presumed that the RNA aptamer modification would contribute to an increase in the R8-mediated pathway.

That the RNA aptamer was attached to the surface of the R8-modified MITO-Porter was confirmed based on physicochemical properties such as ζ potentials (Table 2). These results indicate that the RNA aptamer coats the entire surface of the R8-modified MITO-Porter, but may not be able to inactivate the R8-mediated pathway. We previously found a similar phenomenon that modification of the R8-modified carriers with hyaluronic acid resulted in a negatively charged carrier surface, while the cellular uptake activity of R8-modified carriers with or without hyaluronic acid were comparable [28]. As an explanation for this, it is possible that the head group of R8 could be displayed on the RNA aptamer coated carrier-surface, and a part of the R8 could then induce cellular uptake.

In this scenario, R8 might be displayed on the MITO-Porter as a topology favorable to cellular uptake by RNA aptamer modification at the optimal amount (2.5 mol%). While, an excess amount of RNA aptamer (4.0 mol%) might mask even the head group of R8 displayed on the RNA aptamer coated carrier-surface, resulting in a decrease in cellular uptake. We presumed that the ratio of RNA aptamer modified on the R8-modified MITO-Porter might affect the cellular uptake activity of R8, although the ζ-potentials of a 2.5 mol% and 4.0 mol% RNA aptamer-modified carriers were comparable (Table 2).

We also observed that a loss of mitochondrial membrane potential resulting from an FCCP treatment largely affected the cellular uptake of the RP/R8-modified MITO-Porter. As shown in Figure 6A, the cellular uptake of the RP/R8-modified MITO-Porter was drastically decreased to about 20 % as the result of the FCCP treatment, while that of the R8-modified MITO-Porter was not affected by the FCCP treatment. Based on these results, we hypothesized that the RP/R8-modified MITO-Porter might use, not only the R8-mediated pathway, but also a yet to be discovered uptake pathway. This unknown uptake pathway might be driven by a certain cell function that is dependent of mitochondrial membrane potential.

The effect of the RNA aptamer on enhancing the cellular uptake of

R8-modified MITO-Porter can be useful in *in vitro* conditions. However, the use of this dual ligand-MITO-Porter in *in vivo* conditions should be carefully considered. The R8-modified MITO-Porter could be recognized by the reticuloendothelial system, because macrophages can recognize carriers with a positive charge. Thus, the enhancement in the cellular uptake activity of R8 by RNA aptamer modification might contribute to enhanced macrophage targeting. While, the dual ligand-modified MITO-Porter with a negative charge might escape from the reticuloendothelial system more easily than positively charged R8-modified MITO-Porter. To clarify this point, we plan to investigate the bio-distribution of the dual ligand-modified MITO-Porter in a future study.

In CLSM analyses, the dual-ligand modified MITO-Porter showed a higher mitochondrial targeting activity than the R8-modified MITO-Porter (Figure 4B), suggesting that the function of the mitochondrial RNA aptamer was to enhance the process in a positive direction. In addition, intracellular observations of the R8-modified MITO-Porter equipped with a non-specific aptamer indicated that a non-specific aptamer failed to enhance mitochondrial targeting of R8-modified MITO-Porter (data not shown). The RP/R8-modified MITO-Porter (about 40%) showed the highest values among all carriers. It was also confirmed that the RP/R8-modified MITO-Porter showed the highest mitochondrial occupancy rate (about 30%) (Figure 4C). The mitochondrial occupancy rate indicates that the level of accumulation of carriers within the mitochondrial region of the total mitochondrial region in a cell, and is used to evaluate the mitochondrial accumulation of the carriers. In the case of mitochondrial related diseases where the cells contain both mutant and wild-type mtDNA (heteroplasmy), when the percentage of mutant mtDNA exceeds a certain threshold level in mitochondria (abnormal mitochondria), mitochondrial dysfunction becomes clinically apparent [29,30]. Accordingly, it would be expected that the delivery of therapeutic molecules to mitochondria in diseased cells would decrease the percentage of abnormal mitochondria, resulting in the suppression of a mitochondrial disease. Thus, the mitochondrial occupancy rate could be an important criteria for evaluating the success of mitochondrial therapy.

To investigate the effect of mitochondrial membrane potential on the mitochondrial targeting of the carriers, their intracellular trafficking was observed in the presence/absence of FCCP (Figure 5A). The results show that mitochondrial targeting by the RP/R8-modified MITO-Porter was drastically inhibited, similar to that of the R8-modified MITO-Porter when the cells were treated with FCCP. It seems reasonable to assume that electrostatic interactions of the positively charged R8 with negatively

charged mitochondria would result in an enhancement in mitochondrial targeting. In the case of the RP/R8-modified MITO-Porter, the head group of R8 displayed on the RNA aptamer coated carrier-surface might contribute to mitochondrial delivery. However, it cannot be concluded that the mitochondrial targeting of the negatively charged RP/R8-modified MITO-Porter is achieved only *via* electrostatic interactions. When the cells were treated with FCCP, the mitochondrial membrane potential was decreased, probably leading to a decrease in ATP production *via* the membrane potential. In such a situation (Figure 5A), mitochondrial ATP production would be decreased as the result of the depression in the mitochondrial membrane potential. Therefore, an FCCP treatment would inhibit the ATP-dependent mitochondrial targeting of RP/R8-modified MITO-Porter.

Moreover, it was confirmed that the mitochondrial targeting by the RP/R8-modified MITO-Porter was significantly decreased by ATP depletion compared with the R8-modified MITO-Porter (Figure 5B). In the case of an oligomycin treatment, the mitochondrial membrane potential was maintained. Therefore, positively charged R8-modified MITO-Porter would exert its effect *via* the mitochondrial targeting pathway *via* the mitochondrial membrane potential more efficiently than the negatively charged RP/R8-modified MITO-Porter. In a previous report, the addition of ATP enhanced the import of tRNA into isolated mitochondria and cellular mitochondria [31,32]. Thus, we conclude that the RP/R8-modified MITO-Porter mainly involved an ATP-dependent mitochondrial targeting pathway.

Based on the obtained data, a model for the intracellular trafficking events of the RP/R8-modified MITO-Porter and R8-modified MITO-Porter is illustrated in Figure 7. The RP/R8-modified MITO-Porter and R8-modified MITO-Porter were internalized into cells *via* macropinocytosis and clathrin-dependent endocytosis. The RP/R8-modified MITO-Porter also involves the use of unknown uptake pathway *via* mitochondrial membrane potential. The cellular uptake values for the RP/R8-modified MITO-Porter and the R8-modified MITO-Porter were determined to be 56 and 28. After cellular uptake, both carriers were targeted to mitochondria. As shown in Figure 5B (e), mitochondrial targeting *via* ATP would largely affect the RP/R8-modified MITO-Porter. The mitochondrial targeting rates for the RP/R8-modified MITO-Porter and the R8-modified MITO-Porter were determined to be 38% and 22%. Modification with RP could facilitate the mitochondrial targeting that is dependent on ATP. Collectively, the RP/R8-modified MITO-Porter accumulates in mitochondria at a 4 fold higher level than the R8-modified MITO-Porter, suggesting that the dual-ligand modified MITO-Porter facilitates cellular uptake and mitochondrial targeting more efficiently than the

R8-modified MITO-Porter.

5. Conclusion

The results presented herein constitute the first report of the use of a mitochondrial RNA aptamer modified nanocarrier system to regulate intracellular trafficking, although lipophilic and cationic peptide-based mitochondrial targeting has been reported in previous studies [12,19,33-35]. In this study, we determined the optimal dual-ligand system for a nanocarrier for achieving efficient cellular uptake and mitochondrial targeting (RP/R8-modified MITO-Porter). However, more improvements in selective mitochondrial targeting are needed, since the mitochondrial occupancy rate was only 30%. We previously reported on the use of RNA aptamers for targeting mitochondria using mitochondria-based systematic evolution of ligands by the exponential enrichment (SELEX) method, which are referred to as Mitomers [36]. Thus, we conclude that Mitomer modification would be a key factor in the selective mitochondrial targeting of nanocarrier in living cells. Studies concerning this are currently underway.

Acknowledgements

This work was supported, in part by, a Grant-in-Aid for Scientific Research (B) (grant 26282131 to Y.Y.) from the Ministry of Education, Culture, Sports, Science and Technology, the Japanese Government (MEXT), the Mochida Memorial Foundation for Medical and Pharmaceutical Research, and the Uehara Memorial Foundation. We also thank Dr. Milton Feather for his helpful advice in writing the manuscript.

References

1. Wallace DC 2012. Mitochondria and cancer. Nature reviews Cancer 12(10):685-698.
2. Chan DC 2006. Mitochondria: dynamic organelles in disease, aging, and development. Cell 125(7):1241-1252.
3. Reeve AK, Krishnan KJ, Turnbull D 2008. Mitochondrial DNA mutations in disease, aging, and neurodegeneration. Ann N Y Acad Sci 1147:21-29.
4. Schapira AH 2006. Mitochondrial disease. Lancet 368(9529):70-82.
5. Zhang E, Zhang C, Su Y, Cheng T, Shi C 2011. Newly developed strategies for multifunctional mitochondria-targeted agents in cancer therapy. Drug Discov Today 16(3-4):140-146.
6. Mukhopadhyay A, Weiner H 2007. Delivery of drugs and macromolecules to mitochondria. Adv Drug Deliv Rev 59(8):729-738.
7. Yamada Y, Harashima H 2008. Mitochondrial drug delivery systems for macromolecule and their therapeutic application to mitochondrial diseases. Adv Drug Deliv Rev 60(13-14):1439-1462.
8. Seibel P, Trappe J, Villani G, Klopstock T, Papa S, Reichmann H 1995. Transfection of mitochondria: strategy towards a gene therapy of mitochondrial DNA diseases. Nucleic acids research 23(1):10-17.
9. Fujino T, Ide T, Yoshida M, Onitsuka K, Tanaka A, Hata Y, Nishida M, Takehara T, Kanemaru T, Kitajima N, Takazaki S, Kurose H, Kang D, Sunagawa K 2012. Recombinant mitochondrial transcription factor A protein inhibits nuclear factor of activated T cells signaling and attenuates pathological hypertrophy of cardiac myocytes. Mitochondrion 12(4):449-458.
10. Flierl A, Jackson C, Cottrell B, Murdock D, Seibel P, Wallace DC 2003. Targeted delivery of DNA to the mitochondrial compartment via import sequence-conjugated peptide nucleic acid. Mol Ther 7(4):550-557.
11. Yamada Y, Harashima H 2013. Enhancement in selective mitochondrial association by direct modification of a mitochondrial targeting signal peptide on a liposomal based nanocarrier. Mitochondrion 13(5):526-532.
12. Kawamura E, Yamada Y, Yasuzaki Y, Hyodo M, Harashima H 2013. Intracellular observation of nanocarriers modified with a mitochondrial targeting signal peptide. Journal of bioscience and bioengineering 116(5):634-637.
13. Wang G, Chen HW, Oktay Y, Zhang J, Allen EL, Smith GM, Fan KC, Hong JS, French SW, McCaffery JM, Lightowlers RN, Morse HC, 3rd, Koehler CM, Teitell MA 2010. PNPASE regulates RNA import into mitochondria. Cell 142(3):456-467.

14. Wang G, Shimada E, Zhang J, Hong JS, Smith GM, Teitell MA, Koehler CM 2012. Correcting human mitochondrial mutations with targeted RNA import. Proc Natl Acad Sci U S A 109(13):4840-4845.
15. Adhya S, Mahato B, Jash S, Koley S, Dhar G, Chowdhury T 2011. Mitochondrial gene therapy: The tortuous path from bench to bedside. Mitochondrion 11(6):839-844.
16. Adhya S, Ghosh T, Das A, Bera SK, Mahapatra S 1997. Role of an RNA-binding protein in import of tRNA into Leishmania mitochondria. J Biol Chem 272(34):21396-21402.
17. Yamada Y, Akita H, Kamiya H, Kogure K, Yamamoto T, Shinohara Y, Yamashita K, Kobayashi H, Kikuchi H, Harashima H 2008. MITO-Porter: A liposome-based carrier system for delivery of macromolecules into mitochondria via membrane fusion. Biochimica et biophysica acta 1778(2):423-432.
18. Yamada Y, Furukawa R, Yasuzaki Y, Harashima H 2011. Dual function MITO-Porter, a nano carrier integrating both efficient cytoplasmic delivery and mitochondrial macromolecule delivery. Mol Ther 19(8):1449-1456.
19. Kajimoto K, Sato Y, Nakamura T, Yamada Y, Harashima H 2014. Multifunctional envelope-type nano device for controlled intracellular trafficking and selective targeting in vivo. J Control Release 190C:593-606.
20. Takara K, Hatakeyama H, Kibria G, Ohga N, Hida K, Harashima H 2012. Size-controlled, dual-ligand modified liposomes that target the tumor vasculature show promise for use in drug-resistant cancer therapy. J Control Release 162(1):225-232.
21. Kibria G, Hatakeyama H, Ohga N, Hida K, Harashima H 2011. Dual-ligand modification of PEGylated liposomes shows better cell selectivity and efficient gene delivery. J Control Release 153(2):141-148.
22. Futaki S, Ohashi W, Suzuki T, Niwa M, Tanaka S, Ueda K, Harashima H, Sugiura Y 2001. Stearylated arginine-rich peptides: a new class of transfection systems. Bioconjug Chem 12(6):1005-1011.
23. Heuser JE, Anderson RG 1989. Hypertonic media inhibit receptor-mediated endocytosis by blocking clathrin-coated pit formation. The Journal of cell biology 108(2):389-400.
24. Hewlett LJ, Prescott AR, Watts C 1994. The coated pit and macropinocytic pathways serve distinct endosome populations. The Journal of cell biology 124(5):689-703.
25. Lamaze C, Schmid SL 1995. The emergence of clathrin-independent pinocytic pathways. Current opinion in cell biology 7(4):573-580.

26. Bakker EP, Van den Heuvel EJ, Van Dam K 1974. The binding of uncouplers of oxidative phosphorylation to rat-liver mitochondria. Biochimica et biophysica acta 333(1):12-21.
27. Linnett PE, Beechey RB 1979. Inhibitors of the ATP synthethase system. Methods Enzymol 55:472-518.
28. Yamada Y, Hashida M, Harashima H 2015. Hyaluronic acid controls the uptake pathway and intracellular trafficking of an octaarginine-modified gene vector in CD44 positive- and CD44 negative-cells. Biomaterials 52:189-198.
29. Holt IJ, Harding AE, Petty RK, Morgan-Hughes JA 1990. A new mitochondrial disease associated with mitochondrial DNA heteroplasmy. Am J Hum Genet 46(3):428-433.
30. Kagawa Y, Inoki Y, Endo H 2001. Gene therapy by mitochondrial transfer. Adv Drug Deliv Rev 49(1-2):107-119.
31. Bhattacharyya SN, Chatterjee S, Adhya S 2002. Mitochondrial RNA import in Leishmania tropica: aptamers homologous to multiple tRNA domains that interact cooperatively or antagonistically at the inner membrane. Molecular and cellular biology 22(12):4372-4382.
32. Rubio MA, Rinehart JJ, Krett B, Duvezin-Caubet S, Reichert AS, Soll D, Alfonzo JD 2008. Mammalian mitochondria have the innate ability to import tRNAs by a mechanism distinct from protein import. Proc Natl Acad Sci U S A 105(27):9186-9191.
33. Weissig V 2011. From serendipity to mitochondria-targeted nanocarriers. Pharmaceutical research 28(11):2657-2668.
34. Weissig V, D'Souza GG, Torchilin VP 2001. DQAsome/DNA complexes release DNA upon contact with isolated mouse liver mitochondria. J Control Release 75(3):401-408.
35. Kawamura E, Yamada Y, Harashima H 2013. Mitochondrial targeting functional peptides as potential devices for the mitochondrial delivery of a DF-MITO-Porter. Mitochondrion 13(6):610-614.
36. Tawaraya Y, Hyodo M, Ara MN, Yamada Y, Harashima H 2014. RNA aptamers for targeting mitochondria using a mitochondria-based SELEX method. Biol Pharm Bull 37(8):1411-1415.

Table 1 Mitochondrial RNA aptamers used in this study

	Nucleotide sequence
Chol-RP	***RP RNA sequence*:** 5′- UCUCCCUGAGCUUCAGG -3′
Chol-MRP	***MRP RNA sequence*:** 5′- AGAAGCGUAUCCCGCUGAGC -3′
Chol-D-arm	***D-arm RNA sequence**:* 5′- GGGACUGUAGCUCAAUUGGUAGAGCAU -3′

Cholesterol covalently linked to the 3′ end of the 2′-OMe RNAs containing the RP RNA sequence, MRP RNA sequence or D-arm RNA sequence.

Table 2 Physicochemical properties of mitochondrial RNA aptamer/R8-modified MITO-Porter

[a] **MITO-Porter-type**	**RNA aptamer and the modification ratio**	**Diameter (nm)**	**ζ-potential (mV)**
R8-modified MITO-Porter	-	134 ± 30	22 ± 13
RP/R8-modified MITO-Porter	1 mol% RP	129 ± 7	11 ± 6
	2.5 mol% RP	161 ± 28	-32 ± 2
	4 mol% RP	119 ± 4	-32 ± 4
MRP/R8-modified MITO-Porter	1 mol% MRP	112 ± 1	29 ± 17
	2.5 mol% MRP	123 ± 9	-31 ± 1
	4 mol% MRP	116 ± 15	-25 ± 12
D-arm/R8-modified MITO-Porter	1 mol% D-arm	117 ± 5	27 ± 15
	2.5 mol% D-arm	143 ± 6	-33 ± 11
	4 mol% D-arm	114 ± 9	-30 ± 10

[a] All types of MITO-Porters were modified with 10 mol% of R8. Data denote the mean ± S.D. (n=3).

Figure 1 Investigation for the effect of RNA aptamer modification on cellular uptake of the R8-modified MITO-Porter

The cellular uptake of the NBD-labeled carrier was evaluated by flow cytometry as follows mean fluorescence intensity (MFI). (A) The values of R8-modified MITO-Porter (closed columns) and R8-unmodified carriers (open columns) are represented as the mean with SEM (n=3-4). **A significant difference was found by the unpaired t-test ($p<0.01$). (B) The cellular uptake values for the R8-modified MITO-Porter equipped with RP, MRP, the D-arm (closed columns) and R8-unmodified ones (open columns) are summarized. Data are represented as the mean with SEM (n=3-4). We performed a two-way ANOVA analysis to compare the effect of multiple levels of two factors that are the "aptamer type" and the "modification ratio of R8/aptamer". ###Significant differences between R8-unmodified carrier and other carriers among "modification ratio of R8/aptamer" ($p < 0.001$ by two-way ANOVA, followed by bonferroni test). There was no significant difference of different "aptamer type" on the cellular uptake value and no interaction between two factors.

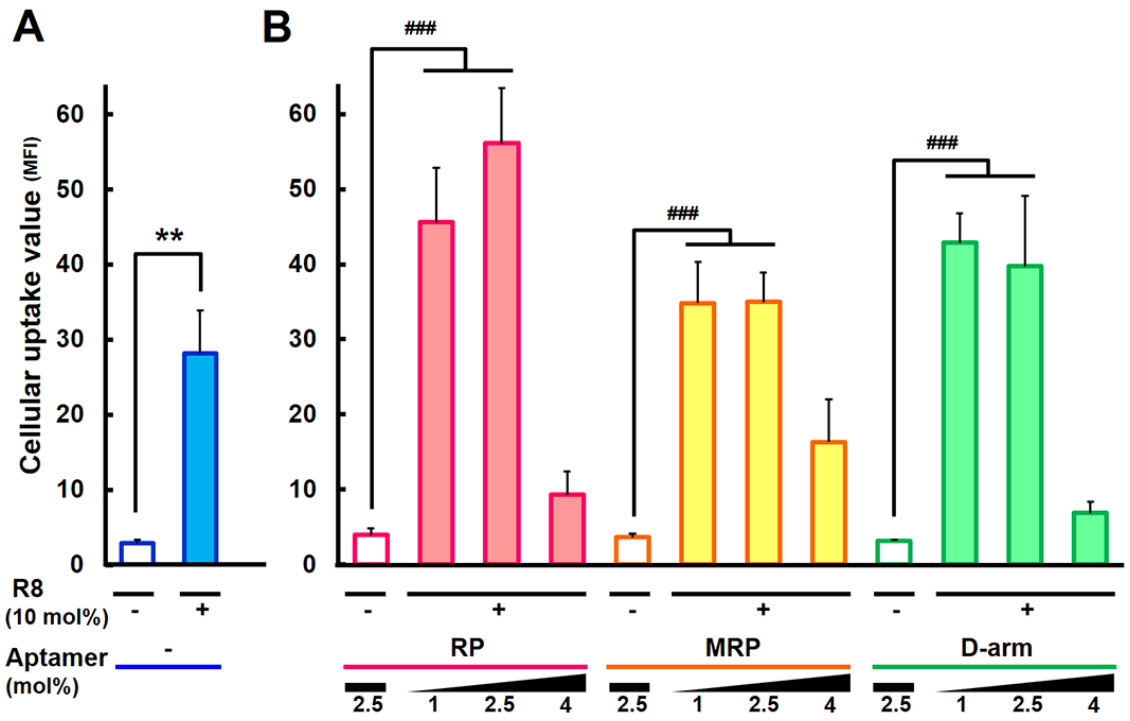

Figure 2 Investigation of cellular uptake pathway of RNA aptamer/R8-modified MITO-Porter

HeLa cells were incubated with the NBD-labeled R8-modified MITO-Porter (A), RP/R8-modified MITO-Porter (B), MRP/R8-modified MITO-Porter (C), D-arm/R8-modified MITO-Porter (D) in the absence (closed bars) and presence (open bars) of sucrose (clathrin-mediated endocytosis inhibitor), amiloride (macropinocytosis inhibitor) or filipin III (caveolae-mediated inhibitor). The mean fluorescence intensity (MFI) of the NBD labeled carriers was measured by flow cytometry, and is expressed as a percent of the MFI in the absence of inhibitors, relative cellular uptake value (%). Data are represented as the mean with SEM (n=3). In each carrier, significant differences between non treatment and others were calculated by one-way ANOVA, followed by bonfferoni test (**p<0.01, *p<0.05).

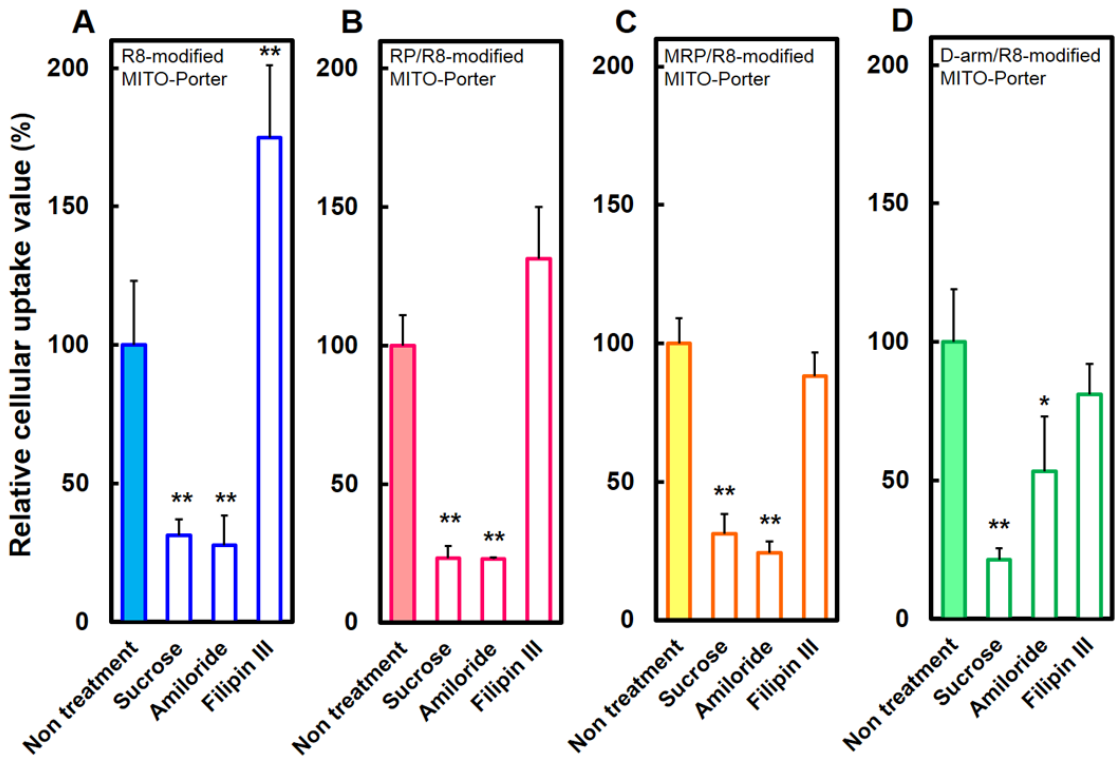

Figure 3 Intracellular observation of RNA aptamer/R8-modified MITO-Porter

HeLa cells were incubated with NBD-labeled MITO-Porter (R8-modified MITO-Porter (A), RP/R8-modified MITO-Porter (B), MRP/R8-modified MITO-Porter (C), D-arm/R8-modifiedMITO-Porter (D)) for 3 h. After staining the mitochondria with Mitofluor 549, the cells were observed by CLSM. NBD-labeled MITO-Porter appeared as yellow clusters when it was localized in mitochondria. Image of b indicates magnification image of interest region in a. Image c indicates a merged image combining a bright field image and a fluorescent image (a). Scale bars; 30 μm.

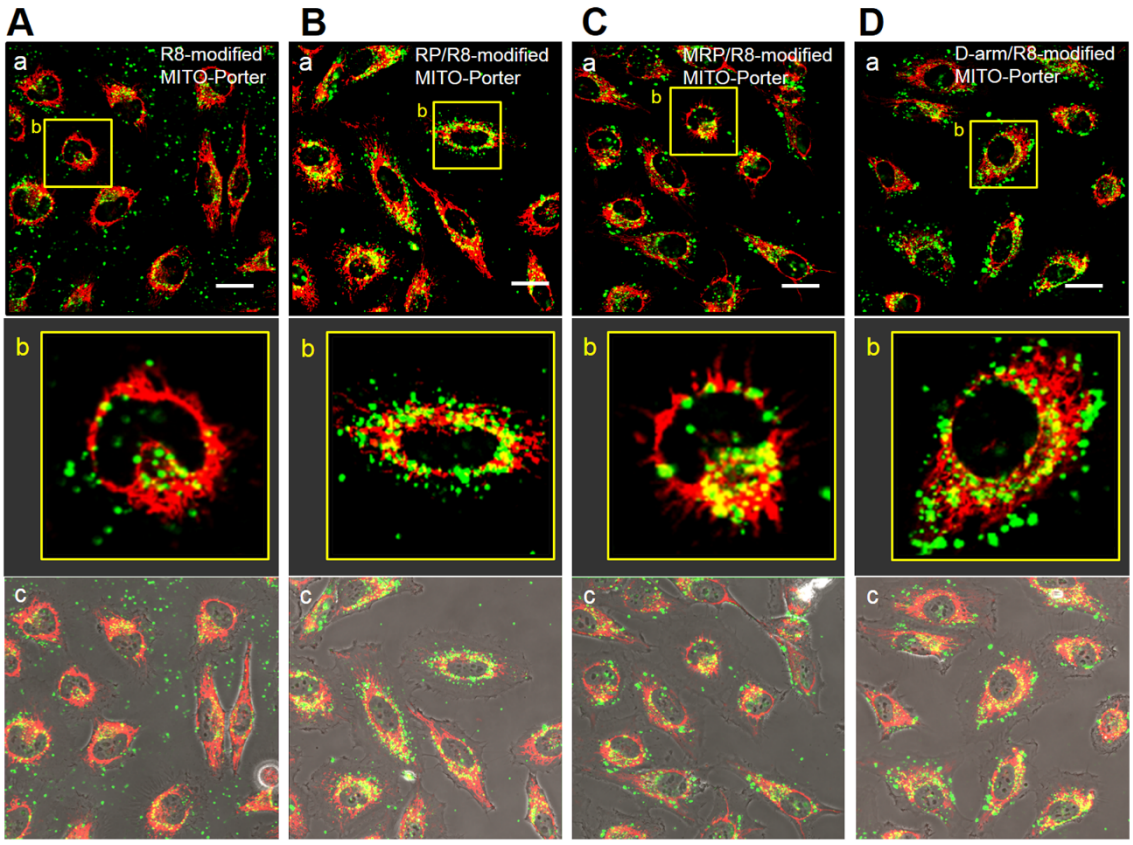

Figure 4 Evaluation of mitochondrial targeting activity and mitochondrial occupancy

A, Schematic image of intracellular observation of carriers and formulation of the mitochondrial targeting rate (1) and mitochondrial occupancy rate (3) based on the CLSM images shown in Figure 3 (see the Materials and Methods for the details). Mitochondrial targeting rate (B) that carriers colocalized with mitochondria of all carriers taken up by the cell and mitochondrial occupancy (C) that the carriers accumulated within the mitochondrial region of the total mitochondrial region in cell are summarized. Circles represent the values of individual cells summarized in each treatment. Bars are the mean value (n=32-39). ***Significant differences between R8-modified MITO-Porter and others were calculated by one-way ANOVA, followed by bonfferoni test ($p<0.001$).

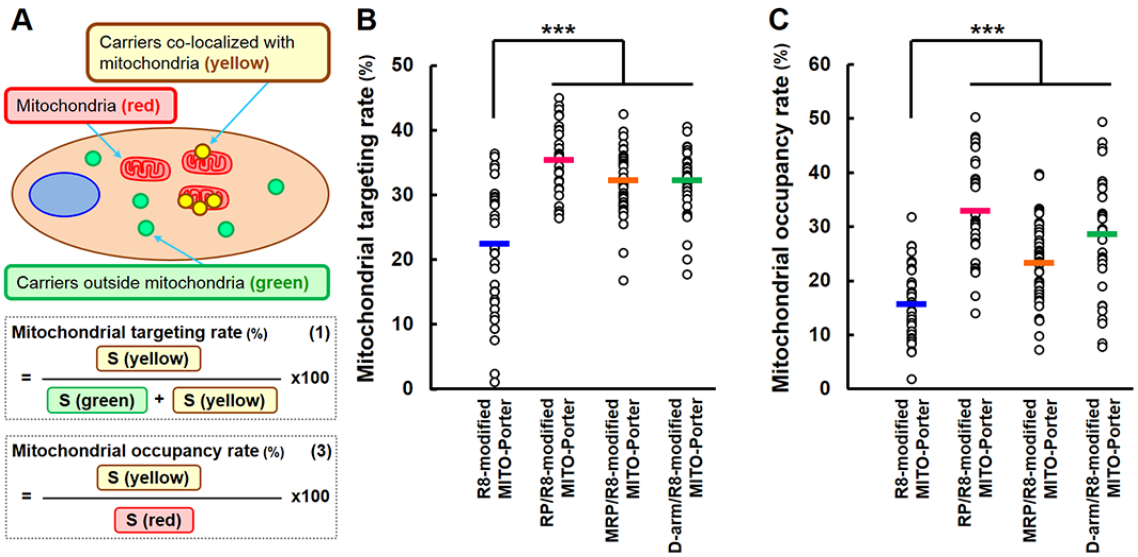

Figure 5 Investigation of the effect of mitochondrial membrane depolarization and mitochondrial ATP loss on mitochondrial targeting of dual-ligand modified MITO-Porter

Intracellular observation of NBD-labeled MITO-Porter (green) after staining mitochondria red in FCCP treatment (a-d in Figure 5A) and oligomycin treatment (a-d in Figure 5B). Scale bars; 30 μm. Relative mitochondrial targeting rates (e) were evaluated based on CLSM image. Data are represented as the mean with SEM (n=22-36). In Figure 5A (e), we performed two-way ANOVA analysis to compare the effect of two factors that are "carrier type" and "FCCP treatment". In Figure 5B (e), we performed a two-way ANOVA analysis to compare the effect of two factors that are "carrier type" and "oligomycin treatment". Since there was significant interaction between two factors, simple main effect test also performed. *** indicate significant differences ($p < 0.001$ by simple main effect test, followed by Bonferroni correction).

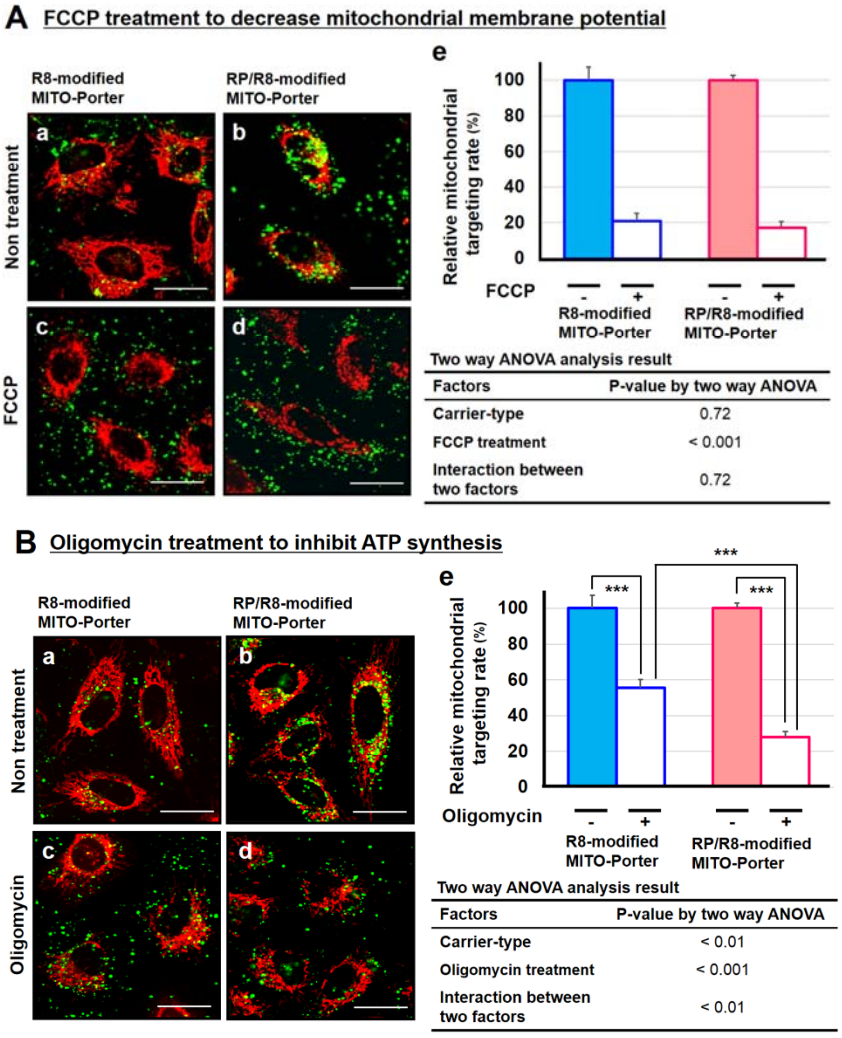

Figure 6 Investigation of the effect of FCCP and oligomycin treatment on cellular uptake of dual-ligand modified MITO-Porter

HeLa cells were incubated with NBD-labeled carriers, and the relative cellular uptake values were evaluated in the presence (closed columns) and absence (open columns) of FCCP (A) or oligomycin (B). Data are represented as the mean with SEM (n=3). **Significant difference was calculated by unpaired t-test ($p < 0.01$).

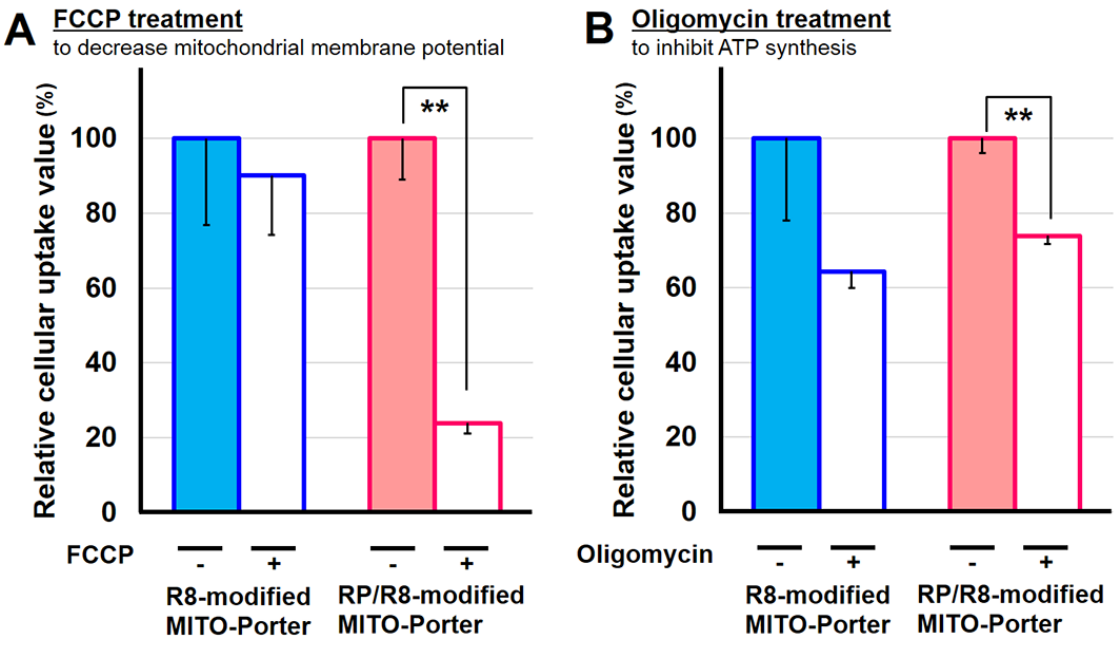

Figure 7 Schematic diagram illustrating the intracellular trafficking events of RP/R8-modified MITO-Porter and R8-modified MITO-Porter.

A model for the intracellular trafficking events of RP/R8-modified MITO-Porter and R8-modified MITO-Porter are shown. The cellular uptake values and mitochondrial targeting rates were quantified based on cellular uptake analyses and CLSM image analyses.

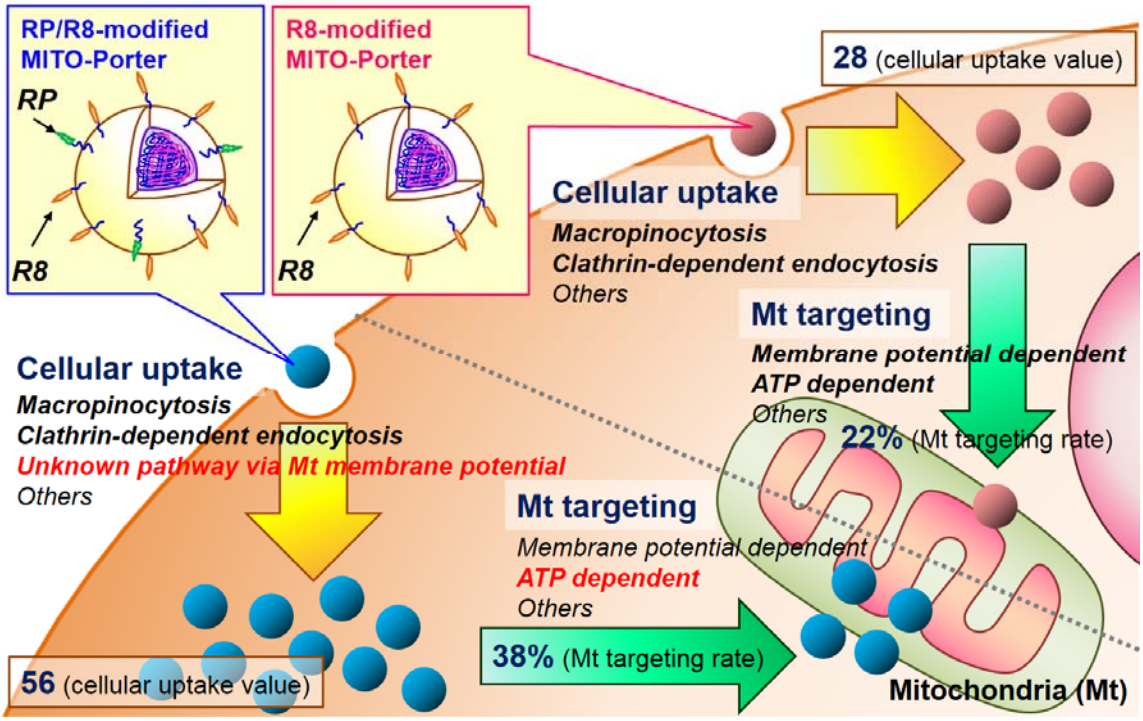

Supplementary data

SUPPLEMENTARY MATERIAL

Figure S1. Merge images of bright field and fluorescent images regarding intracellular observation of MITO-Porter in FCCP treatment.

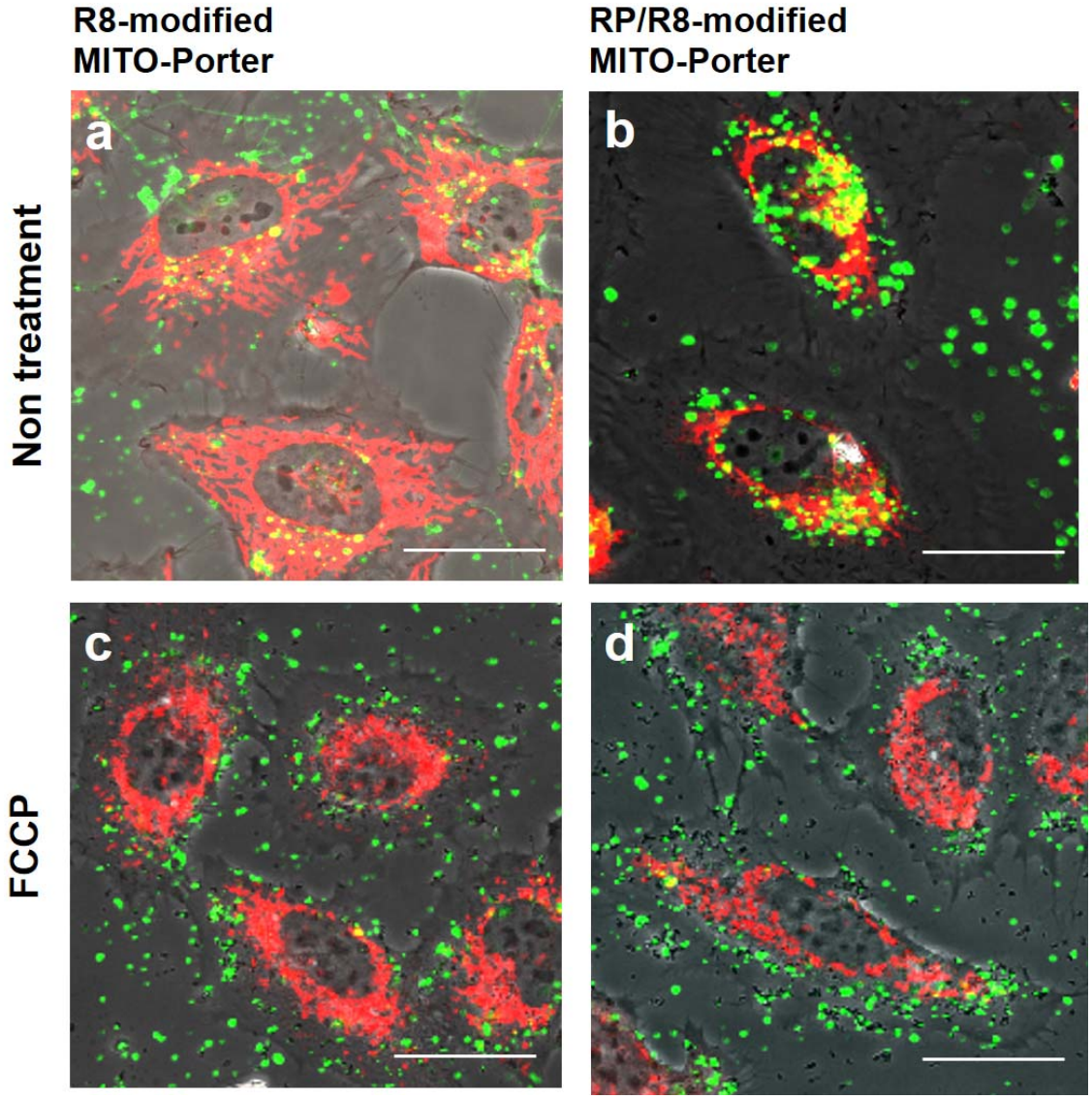

Intracellular observation of NBD-labeled MITO-Porter (green) after staining mitochondria red in FCCP treatment (a-d). These images were made using fluorescent images of Figure 5A (a-d). Scale bars; 30 μm.

Figure S2. Merge images of bright field and fluorescent images regarding intracellular observation of MITO-Porter in oligomycin treatment.

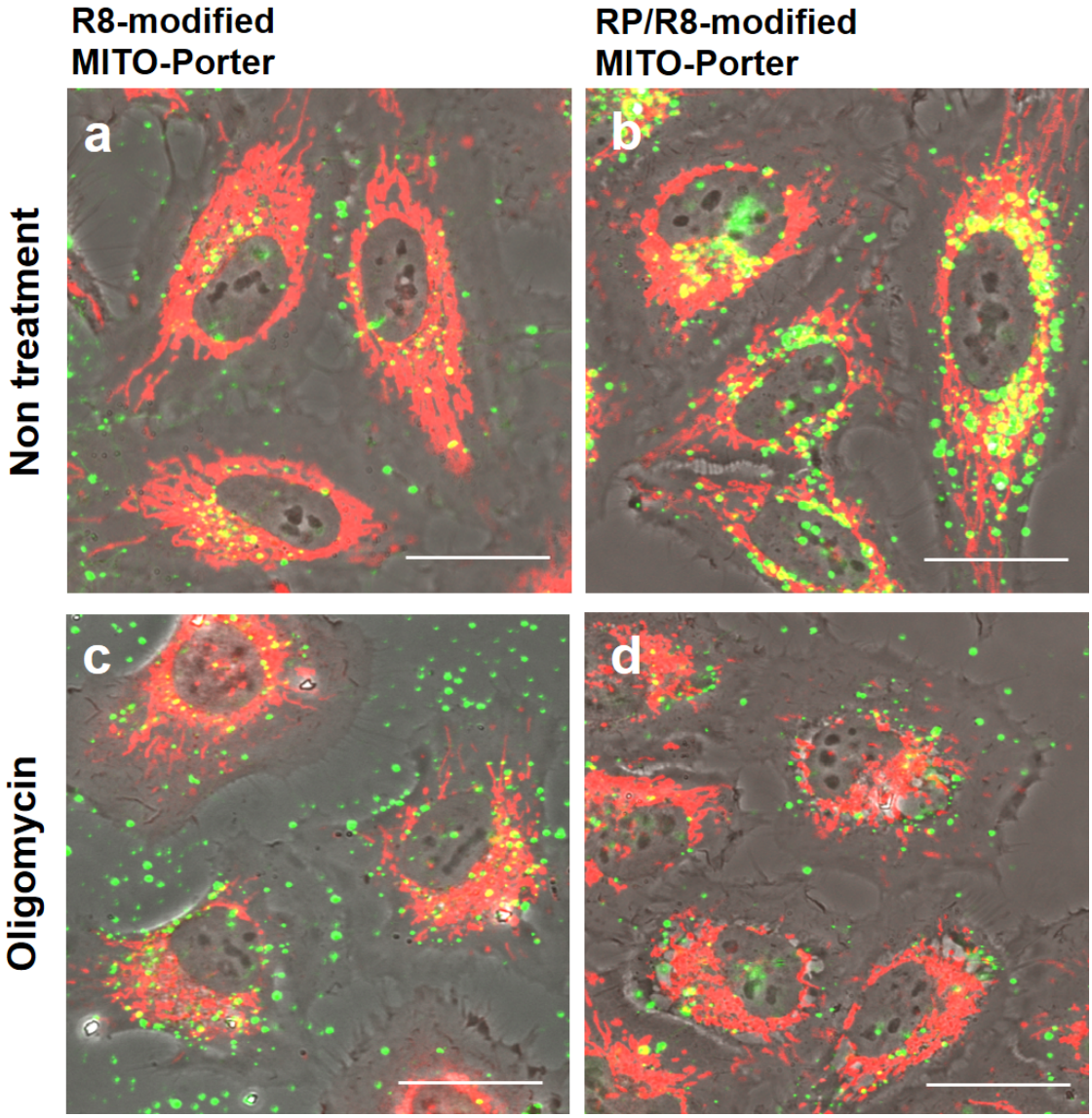

Intracellular observation of NBD-labeled MITO-Porter (green) after staining mitochondria red in oligomycin treatment (a-d). These images were made using fluorescent images of Figure 5B (a-d). Scale bars; 30 μm.